This article has been accepted for publication in a future issue of this journal, but has not been fully edited. Content may change prior to final publication. Citation information: DOI 10.1109/JSEN.2019.2908312, IEEE Sensors Journal



# Portable Electromyography: A Case Study on Ballistic Finger Movement Recognition

Ala Shaabana, Joey Legere, Jun Li, Rong Zheng, Martin V. Mohrenschildt, Judith M. Shedden

***Abstract*—In neuromuscular analysis, electromyography (EMG) is typically used to analyze aggregate Action Potential (AP) signals to detect medical abnormalities, activation levels, recruitment order, or analyze biomechanics. In our previous work, we compared the performance of these off-the-shelf solutions to research-grade EMG machines and found that due to their rigid electrode placement, low sampling rate, and data transmission medium they are ill-suited for research use, in which data collection must be robust and accurate. We present XTREMIS: a low-cost and portable EMG platform with a small form factor (55mm x 35mm) that has a sample rate comparable to research-grade EMG machines. Indeed, experiments on 8 subjects have shown that not only does XTREMIS functionally outperform technologies; its signal quality is high enough to achieve finger movement classification accuracy similar to research-grade EMG machines, making it a suitable platform for research.**

***Index Terms*—Electromyography, Wearable Technology, Gesture Recognition, Gaussian Mixture, Hidden Markov Model**

## I. Introduction

Electromyography (EMG) is an electro-diagnostic tool used to analyze muscle response or electrical activity in response to a nerve's stimulation of the muscle. This is done by detecting a small bioelectric pulse called the Action Potential (AP) that is generated when muscles contract and relax. By analyzing the AP signal, it becomes possible to analyze medical abnormalities, activation levels, muscle recruitment order, or biomechanics [1]. Currently there exist two types of EMG: intramuscular EMG and surface EMG (sEMG). Intramuscular EMG requires an electrode to be inserted into the muscle that is being measured. This is an invasive process and can be painful to the person being measured, however the signal is typically clear with a low amount of noise. On the other hand, surface EMG electrodes are placed on the skin, making it non-invasive and pain-free. However, the signal is noisy and requires proper filtering before being processed.

There has been a myriad of research on the use of sEMG to drive an actuation based on human biosignals in the past couple of decades. Specifically, sEMG signals are processed and input into classifiers to create functions ranging from hardware control to gesture recognition. Indeed, one of the earliest concepts of using EMG for robotics control was proposed by Farry *et al.* in 1996, in which they proposed converting EMG signals into commands for NASA/Johnson Space Center's sixteen degree-of-freedom Utah/MIT Dexterous Hand for two grasping (key and chuck) options and three thumb motions (abduction, extension, and flexion) [2]. As of late, EMG research has been more focused on the classification of intricate tasks. This naturally led researchers to finger movement classification. In 2013, Chen *et al.* proposed a pattern recognition system to perform automatic classification on multiple finger movements, specifically Chinese sign language gestures for numbers ranging from 0 to 9 [3]. Moreover, they investigated the effects of different feature and classifier combinations in offline recognition, and have taken a further step by implementing a real-time recognition system with above 90% accuracies for all subjects.

Due to advances in integrated circuit technology and the ease of use of surface electrodes, developers have begun to integrate sEMG technology into wearable devices for various applications ranging from gesture recognition [4] to fitness assessment [5], [6]. In 2017, we investigated the possibility of recognizing ballistic gestures – repetitive, spontaneous propulsions of the limbs in activities such as playing instruments or typing – using two different EMG devices. Specifically, we evaluated the performance of a Myo gesture recognition armband [4] against a Biosemi ActiveTwo research-grade EMG machine [7] and found that while the BioSemi ActiveTwo achieved a high classification accuracy, the Myo armband suffers from two significant setbacks that prevented it from achieving a high classification performance [8]:

1) **Rigid electrode placement**: The electrodes can only be placed in one specific way on pre-specified muscles fitting the primary application of the device. For example, Myo's primary purpose is gesture recognition, and hence it can only be placed on forearm muscles near the elbow [4].
2) **Limited sampling rate**: Due to power constraints, maximum device sampling rates are typically at approximately 200 Hz. Significant information in the signal may be lost as this does not satisfy the Nyquist-Shannon sampling theorem as typical aggregate muscle motor unit action potential is usually between 10 Hz and 500 Hz [9].

However, the high costs and complexity of research-grade EMG machines prevent developers and scientists without an electronics engineering background from utilizing them for their research needs, instead resorting to off-the-shelf wearable devices like Myo. Thus, we present XTREMIS: a low-cost, portable, and powerful hardware and software solution to EMG data collection. XTREMIS is an EMG data collection device with an adjustable biomedical instrumentation chip and flexible electrode placement. In order to evaluate the validity and performance of XTREMIS, two types of experiments were performed: finger movement recognition and a signal-level analysis and similarity measure. The performance of XTREMIS is also compared against the BioSemi ActiveTwo and the Myo armband. Thus, our contribution in this paper is five-fold:

1) We present XTREMIS: a hardware platform and software solution for Electrocardiography (EKG), Electromyography (EMG), and Electroencephalography (EEG) data collection.
2) We propose a Gaussian mixture Hidden Markov model (GM-HMM) to classify ballistic gestures during a typing task.
3) We present a detailed evaluation of the different factors that affect finger movement classification during typing, namely: speed of typing, placement of electrodes on the skin, and sampling rates.
4) We perform a signal-level analysis on XTREMIS and compare its performance to a research-grade EMG machine.

Authors' addresses: A. Shaabana, J. Legere, J. Li, R. Zheng, M. v. Mohrenschildt, Department of Software and Computing, McMaster University, 1280 Main Street West, Hamilton, ON L8S 4K1, Canada; J. Shedden, Department of Psychology, Neuroscience, and Behaviour, McMaster University, Hamilton, ON L8S 4K1, Canada

Preliminary version of portions of this paper appeared in *IEEE IEEE/ACM Conference on Connected Health: Applications, Systems, and Engineering Technologies*

This article has been accepted for publication in a future issue of this journal, but has not been fully edited. Content may change prior to final publication. Citation information: DOI 10.1109/JSEN.2019.2908312, IEEE Sensors Journal



5) We evaluate the performance of both devices in classifying ballistic gestures using a Gaussian Mixture Hidden Markov Model (GM-HMM).

The rest of this paper is organized as follows: Section II discusses gesture recognition and previous works. Section III discusses the hardware design and software architecture of XTREMIS. Section IV details the GM-HMM applied in recognizing finger movements in the classification performance evaluation of XTREMIS. Section V highlights the evaluation results of the classifier performance using XTREMIS v.s. a research-grade EMG machine and presents a signal comparison between the two devices. Finally, Section VII presents the conclusion and future works, respectively.

## II. Background and Related Work

Gesture recognition is a problem that has been tackled using many approaches by researchers since the 1990s. However, due to the variety of possible gestures performed by hands, gestures can be identified in two types:

1) *General gestures*: gestures involving the movement of the entire hand or flexing of the fingers such as sign language.
2) *Ballistic gestures*: gestures involving spontaneous propulsion of the limbs in a continuous manner, such as typing.

Further, gesture recognition literature is typically approached using: vision-based or EMG-based. Vision-based gesture recognition involves using a vision-based sensor (regular camera, kinect sensor, etc.) trained at the user's hands to treat them as objects, then features are extracted and sent to a classifier. Image processing techniques such as analysis and detection of shapes, contours, textures, segmentations, motions, and colors have been utilized and found to be effective [10], [11]. However, vision-based approaches are plagued by privacy and granularity concerns. Privacy involves user concerns with regard to how the recorded media is being utilized besides for purposes of data collection. Granularity is concerned with the level of resolution required to recognize subtle or quick gestures such as finger movements. Further, the physical background of the user is also an issue as it may dilute the image and hinder recognition. On the other hand, sensor-based gesture recognition techniques utilize inertial measurement and EMG sensors to extract features and detect gestures. Sensor-based gesture recognition largely solves the privacy issue as an ocular view of the user is not required, unless they do not wish for their muscular data to be shared. However, movement classification still remains problematic with ballistic gestures since they – by nature – involve rapid movements.

Various EMG solutions to general gesture recognition have been developed using a combination of custom hardware and software. One of the earliest works on the application of EMG on Human Computer Interfaces was proposed in 1998 by Rosenberg in which a graphic input device controlled by the wrist is constructed. The device detects the EMG signal of the forearm muscles used to move the wrist and moves the mouse pointer on a screen accordingly. Rosenberg reports that the pointer performs 14% as well as a regular computer mouse at simple pointing tasks [12]. In 2009 Gopra *et al.* proposed an EMG based control method for an upper-limb motion assisting exoskeleton (SUEFUL-7) with 7 degrees of freedom [13]. SUEFUL-7 takes advantage of the EMG signal amplitudes produced by the upper-arm and forearm muscles to predict the intended movement of the wearer. Experiments have shown that the system is effective in helping physically weak individuals to rotate their shoulders and extend/flex their wrists [13].

Chen *et al.* proposed a pattern recognition system to perform automatic classification on multiple finger movements, specifically Chinese sign language gestures for numbers ranging from 0 to 9 [3]. The proposed hardware system consisted of an instrumentation amplifier and two TelosB motes as an analog-to-digital converter and to wirelessly transmit data. Although their design is compact, each channel requires two electrodes at a time — one reference and one channel electrode. This design fits their implementation with 4 channels [3] but quickly becomes cumbersome when dealing with high electrode counts such as 8 or 16. XTREMIS resolves this issue by using one common reference electrode that works with each channel individually, eliminating the clutter.

Pareschi *et al.* designed an analog-to-information converter based on compressed sensing that acquires biosignals with Nyquist frequency up to 100kHz [14]. Compressed sensing is utilized to reduce the amount of data necessary to represent the signal information content. Further, the proposed system contains signal saturation checking mechanisms to allow users to reconstruct the input signal regardless of the presence of saturation with minimal hardware requirement costs. Experiments on biomedical signals show that the prototype is capable of successfully acquiring signals with high compression factor [14].

### A. Muscular Physiology

Instead of being controlled with interior muscles, human fingers function in a pulley system powered by the forearm. In fact, there are 20 muscles in the forearm that control fingers and movement. They can be divided into 2 types: extrinsic and intrinsic muscles. The extrinsic muscles are the long flexors and extensors. The flexors are located on the underside of the arm, and allow for the bending of the fingers [15]. The thumb has one long flexor and one short flexor, as well as other muscles to make grasping possible. The extensors, on the other hand, are located on the back of the forearm and they help to straighten fingers out (i.e. finger extensions).

The Flexor Digitorum Profundus' primary functions are the flexing of the wrist, the metacarpophalangeal joints (joints between the bones and phalanges of the fingers), and the interphalangeal joints (hinge joints between the phalanges of the hand). In other words, it helps in flexing the medial four digits of the hand (the index, middle, ring, and pinky fingers). Whereas the Flexor Pollicis Longus muscle serves to primarily flex the thumb. Meanwhile, the Extensor Digitorum Communis muscle allows for the extension of the medial four digits of the hand. Located on the back of the forearm, this muscle is in a constant state of contraction when typing due to the posture of human beings when typing.

## III. Hardware Design

The high-level user flow of XTREMIS is shown in Figure 1. Commands are sent from a computer connected to the same wireless network as XTREMIS. They are then received by the WiFi system-on-chip(SoC) and sent to the processor. The processor, in turn, converts the commands to bytes and sets or clears flags on the 6-degree Inertial Measurement Unit (IMU) or biomedical instrumentation ADC (BIADC) as required. During data collection, the incoming digital signal from the BIADC is timestamped by the processor and converted to hexadecimal format. It is then either saved to the SD card, sent to the WiFi SoC for transmission, or both.

Figure 2 is a picture of the XTREMIS board with the highlighted components as shown in Figure 1. XTREMIS' compact form factor makes it suitable for a wide range of applications: from wearable technology to on-the-fly gesture recognition. The architecture of the XTREMIS board is shown in Figure 3. For simplicity, we split the circuit into two sub-circuits: data acquisition and data processing.

This article has been accepted for publication in a future issue of this journal, but has not been fully edited. Content may change prior to final publication. Citation information: DOI 10.1109/JSEN.2019.2908312, IEEE Sensors Journal



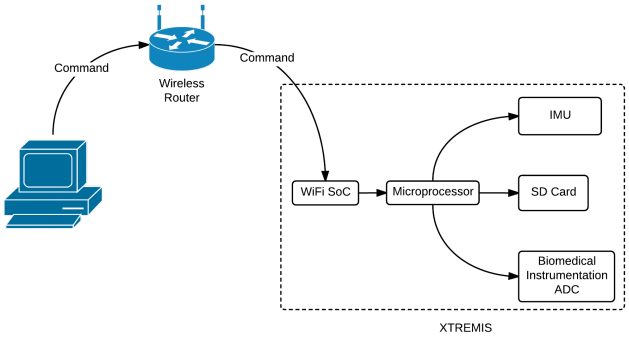


Fig. 1: Information flow of XTREMIS. Commands are sent through WiFi to the WiFi SoC of XTREMIS.

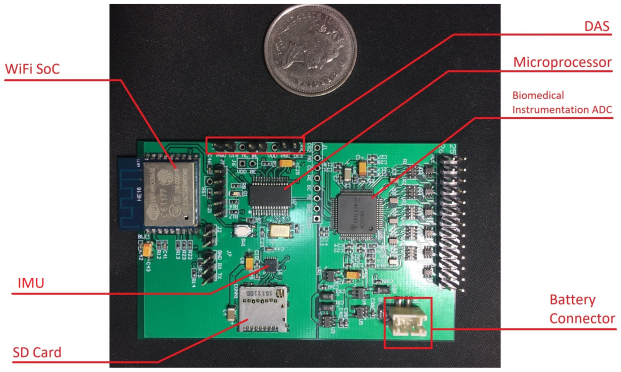


Fig. 2: XTREMIS Circuit Components.

### A. Data Acquisition Circuit (DAC)

Input to the BIADC is collected from 8 individual channels (*S = C1,...,C8*), a Stimulus, Reference, and Bias (SRB) channel, and a BIAS channel. EMG is not an absolute measure, instead it can be considered a relative measure. Based on voltage value of EMG, we cannot compare directly between muscles or between people. Therefore, EMG measurements require a reference electrode to each electrode, the difference between the two is considered the target muscle's voltage. The SRB channel serves, therefore, as a common reference to all channels in S against which the impedance on the skin is measured between it and a given channel.

As for the BIAS channel, the human body acts as an antenna for a wide range of radiation frequencies – including frequencies coming from electrical appliances in the 50 Hz or 60 Hz range – therefore the BIAS channel (also called Driven Right Leg or DRL) takes a copy of the 50 Hz or 60 Hz radiation surrounding the human body and drives it with a scaled, inverted version, effectively canceling it out. It is typically utilized for EEG applications as the signal is weak. The signal for EKG and EMG is stronger and hence it is not required. The BIAS channel input was added to XTREMIS for potential EEG applications in future works.

All channels are first passed through an electrostatic discharge (ESD) protection circuit to protect the BIADC from any electrical shorts with any object that comes into contact with the channel pins. Specifically, a TI TPD4E1B06 4-channel bi-directional transient voltage suppressor was used in our case.

Signals are fed into the BIADC for conversion to digital. First, incoming signals are fed to a voltage divider to reduce their voltage. XTREMIS utilizes a Texas Instruments ADS1299 chip for the BI-ADC due to its ability to process EKG, EMG, and EEG signals with minimal adjustments. Once the analog signal has been converted to a digital one by the BIADC, it is ready for actuation by the data processing circuit.

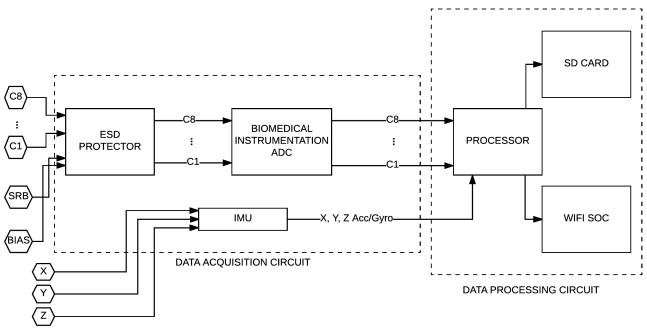


Fig. 3: High-level view of XTREMIS' architecture.

### B. Data Processing Circuit (DPC)

While the DAC is responsible for converting biosignals from analog to digital, the DPC is responsible for the application program interface (API) of XTREMIS as well as processing user commands. More specifically, a 32-bit Microchip PIC32MX250F128B processor is responsible for saving, transmitting, and annotating the data as well as adjusting the settings of the BIADC as per the user's commands coming in from the WiFi SoC. Communications between the actuation components (BIADC, IMU, and SD card) and the processor are done through Serial Peripheral Interface (SPI) protocol so as to handle the high sampling rates that the BIADC and IMU (which contains both a gyroscope and an accelerometer) are capable of.

On the other hand, the WiFi SoC has its own embedded processor and as such communication with the on-board microprocessor was chosen to be Universal Asynchronous Receiver-Transmitter (UART) protocol due to its asynchrony. Synchronization and timing information is embedded into the data stream and synchronization at each end is achieved with a protocol that incorporates start and stop bits. Further, using UART simplifies the design when using streaming-mode: the processor simply dumps the samples collected onto the UART bus and the WiFi SoC picks them up and transmits them. Utilizing UART instead of SPI in this case is namely a design choice it is sufficient to support the high data rates coming from the IMU and the BIADC, thus SPI was not necessary. Finally, the WiFi SoC is programmed independently from the on-board microprocessor, making the programming of XTREMIS a two-step process.

### C. Data Marking System (DMS)

As with any data collection system, it is paramount that the data can be properly marked and annotated in real time if there is a need for it. Certain tasks like typing cannot simply be marked manually, and require a low latency data marking system to properly mark the ground truth data. Past works and current products lack DMS circuits, making the data collection and training process for machine learning applications cumbersome. Due to the nature of biosignals, it is impossible to mark data without an external device. Data marking is usually performed with a video recording of the subject performing and then cross-referencing it with the biosignal data. The DMS in XTREMIS allows for the marking of data "on-the-fly" – that is, as it is being recorded in real time. The inspiration of the DMS

This article has been accepted for publication in a future issue of this journal, but has not been fully edited. Content may change prior to final publication. Citation information: DOI 10.1109/JSEN.2019.2908312, IEEE Sensors Journal



of XTREMIS came from trying to mark the data coming from a research-grade EMG machine in our previous work [8]. To resolve this, we constructed a DMS (referred to as a trigger mechanism) using an Arduino and a PS/2 keyboard that interfaced with the EMG machine to properly mark the data when a key was pressed and when it was released.

XTREMIS employs a similar mechanism in which 6 pins are dedicated as input pins, who's state determines whether or not there needs to be a marking on the data (they are always defaulted to 0 when there is no incoming marker). The reason for using 6 pins (which correspond to 6 bits in software) is to allow a high variability in possible marking mechanisms. Specifically, 6 bits allows us to mark ASCII characters from $0x20$ (space bar) to $0x5F$ (underscore), encompassing all numbers and uppercase letters. If one of the pins' states is set to 1, then the data is marked in that instance and the states are cleared until the next change. This makes it simple to attach any trigger mechanism to any or all of the pins on XTREMIS that changes the states of the pins appropriately according to an action taken by a user, thereby simplifying the collection of data.

## IV. Classification Task

Raw EMG signals come in a somewhat useless form. It hence becomes important to preprocess and analyze them before training a classifier. The raw signal is first cleaned up, and relevant segments of the clean signal are then extracted. Features are then extracted and used in training or invoking a classification.

### A. Preprocessing and Windowing

The first stage that EMG signals have to go through is data preprocessing. The ISEK Standards of Reporting EMG Data states that the firing rate of Motor Unit Action Potentials (MUAP) is typically between 10 Hz and 500 Hz [9], and as such the EMG data is first passed through a bandpass filter within 10 Hz and 500 Hz. In regular gesture recognition systems the next step is usually segmentation, which involves separating inactive periods from active periods in the signal. Active periods are defined as blocks in the time-series signal where muscle contractions are happening, while inactive periods are blocks where the muscle is relaxed. However in ballistic gestures resting periods are very brief or sometimes non-existent. Instead, they become *transition* periods, which are times where the finger is moving from a key release to the next key press. Since transition periods vary in intensity across people and typing speeds, we use overlapping windows to label the onset of key press, period where the key is pressed, and key release.

In regular gesture recognition literature, there are several approaches to segment EMG signals [3], [17], [18], [19], the most common of which are:

1) Segmentation by detecting peaks of Motor Unit Action Potentials (MUAPs).
2) Segmentation using energy/peak detection.
3) Segmentation using Discrete Wavelet Transforms.

Although their performance is good when applied to regular gesture recognition, a caveat of the above methodologies is that they require calculation of parameters such as thresholds, Maximum Voluntary Contraction (MVC), and appropriate window sizing, usually found using trial-and-error in experimentation. Further, using thresholding may be counter intuitive as the instability of signals may create inconsistencies between the shapes of active and transition periods. Although the peaks in the waveform are evident, the fluctuations of rest periods makes it difficult to detect them reliably. These fluctuations are referred to as "movement epenthesis", which occur when performing rapid movements. This is common when dealing with ballistic gestures due to the spontaneity of the gestures and their similarities to a muscle twitch, making them difficult to remove completely using only filters. Finally, thresholds are likely to differ when applied to different people as everyone has different physiologies due to factors like the amount of body fat they have and their muscular structure. Hence, the period between a key release and the next key press cannot be treated as a resting period. Instead, using overlapping windows to label onsets, offsets, and transitions between keys will help to build more robust classifiers. Features are then extracted from each window and the corresponding label that is within it (i.e. a key press, release, or in between a press and a release) is used as the ground truth.

### B. Windowing

When extracting data for training, a sliding window approach with overlap was adopted in which if a key press marker is found then that window and all subsequent windows until the key release marker are labeled with the finger mapped to that key. A sliding window-style of labeling gives information as to how long finger presses and transitions are, making it more resilient to typing speeds. Additionally, sliding windows allow for training the HMM to detect onsets and offsets of key presses, making it more resilient to movement epenthesis – a common phenomenon when dealing with ballistic gestures that occurs due to the spontaneity of the gestures and their similarities to a muscle twitch, making them difficult to remove completely using a filter [8].

### C. Feature Extraction

Once windows of the signal have been identified, features are extracted from each window. The features selected in this work were handpicked from past gesture classification work [20], [3], [21], [22] on fine-grained gesture recognition such as playing the piano [20] and sign language [3]. Alternatively, a random-forest classifier can be used to find the best performing features. Two types of features were extracted: time domain (TD) features and frequency domain (FD) features.

*1) Time Domain Features:* Some of Hudgin's feature set was utilized to obtain the time domain features due to the simplicity of their computations and their ability to describe the signal at the time domain well [21]. In this work, four of these features were implemented in addition to the Root Mean Square.

1) *Mean Absolute Value (MAV)* — Estimate of the MAV of the signal in window $i$ which is $N$ samples in length, given by:

$$\text{MAV}_i = \frac{1}{N}\sum_{k=1}^{N}|x_k^i| \quad \text{where } i = 1, ..., I \tag{1}$$

where $x_k^i$ is the $k^{th}$ sample in window $i$ and $I$ is the total number of windows over the entire signal.

2) *Difference MAV* — Represents the difference in MAV between the window $i$ and the subsequent window $i+1$, given by:

$$\Delta\text{MAV}_i = \text{MAV}_{i+1} - \text{MAV}_i. \tag{2}$$

3) *Slope Sign Changes (SSC)* — Number of times the slope of the waveform changes signs (from positive to negative, or vice versa). A suitable threshold must be chosen to reduce noise induced changes. Given three consecutive samples in window $i$: $x_{k-1}^i$, $x_k^i$, and $x_{k+1}^i$, the slope sign change count is incremented if:

This article has been accepted for publication in a future issue of this journal, but has not been fully edited. Content may change prior to final publication. Citation information: DOI 10.1109/JSEN.2019.2908312, IEEE Sensors Journal



$$\left(x_k^i > \max(x_{k-1}^i, x_{k+1}^i) \quad \vee \quad x_k^i < \min(x_{k-1}^i, x_{k+1}^i)\right) \wedge \quad \max(|x_{k+1}^i - x_k^i|, |x_k^i - x_{k-1}^i) > \Omega, \tag{3}$$

where $\Omega$ is a threshold value that is determined as 0.02mV for a noise value of $21.34\mu$V peak-to-peak [23].

4) *Waveform Length (WL)* — The cumulative length of the waveform over the window $i$. This is the cumulative length of the waveform over the time window, defined as:

$$\text{WL}_i = \sum_{k=2}^{N} \left| x_k^i - x_{k-1}^i \right|, \tag{4}$$

where $x_k^i - x_{k-1}^i$ is the difference in consecutive sample voltages [21].

5) *Root Mean Square (RMS)* — Provides a measure on the power of the signal in window $i$ which is $N$ samples in length.

$$\text{RMS}_i = \sqrt{\frac{1}{N} \sum_{k=1}^{N} (x_k^i)^2}. \tag{5}$$

*2) Frequency Domain Features:* The frequency domain features used were Hjorth's parameters, the mean, and median frequencies extracted from the power spectrum of the signal. Hjorth's parameters are normalized slope descriptors typically used in EEG processing for data reductions or automatic sleep stage scoring. In this work we use them for the detection of the transient EMG signal which occurs during muscle contractions, or when a muscle is switching from a relaxed to a contracted state and vice versa. We first define the spectral moments over a discrete fourier transform. The zero-order moment $m_{0_i}$ over window $i$ is proportional to the mean energy in that window, and is defined as:

$$m_{0_i} = \frac{1}{F} \sum_{f=f_1}^{f_2} P_f^i, \tag{6}$$

where $f_1$ to $f_2$ are a range of frequencies of length $F = f_2 - f_1$, and $P_x^i$ is the discrete power spectrum of the signal in window $i$. Since the EMG frequency range is between 10Hz and 500Hz [9], the range $f_1 = 0$ and $f_2 = 500$ were used. The first-order moment is defined as:

$$m_{1_i} = \frac{1}{F \cdot m_{0_i}} \sum_{f=f_1}^{f_2} P_f^i \left(\frac{f}{N_i \Delta t}\right), \tag{7}$$

where $N_i$ is the length of the power spectrum, and $\Delta t$ is the sampling interval. To get higher order shape information one needs to define the central moments in the discrete domain as follows:

$$m_{n_i} = \frac{1}{F \cdot m_{0_i}} \sum_{f=f_1}^{f_2} P_f^i \left(\frac{f}{N_i \Delta t} - \bar{f}\right)^n, \tag{8}$$

where $\bar{f}$ is the normalized value found from the discrete first order moment. Now that the spectral moments have been defined, we can proceed to defining the Hjorth parameters:

1) *Activity* — Represents signal power as the variance of the amplitude of the signal. In the frequency domain, it can be conceived as the envelope of the power spectrum [24] in window $i$. Activity is defined as:

$$\text{Activity}_i = m_{0_i} = \sigma_{0_i}^2, \tag{9}$$

where $\sigma_{0_i}^2$ is the variance of window $i$.

2) *Mobility* — measures the ratio between the standard deviation of the slope and the standard deviation of the amplitude per time unit. In other words, it represents dominant frequency. Mobility for window $i$ is defined as:

$$\text{Mobility}_i = \sqrt{m_{2_i}/m_{0_i}} = \sigma_{1_i}/\sigma_{0_i}, \tag{10}$$

where the second order moment $m_{2_i}$ is a measure of the width of the spectrum about the mean in window $i$, and $\sigma_{1_i}$ is the standard deviation of the first derivative of the signal in window $i$.

3) *Complexity* — Represents change in frequency. It compares the signal's similarity to a pure sine wave [24], and is defined as:

$$\text{Complexity}_i = \sqrt{(m_{4_i}/m_{2_i}) - (m_{2_i}/m_{0_i})} = \frac{\sigma_{2_i}/\sigma_{1_i}}{\sigma_{1_i}/\sigma_{0_i}}, \tag{11}$$

where $\sigma_{2_i}$ is the standard deviation of the second derivative of window $i$.

Finally, we obtain the mean and median frequencies from window $i$ as follows:

1) *Mean Frequency* — an average frequency which is calculated as the sum of the product of the EMG power spectrum and frequency divided by the total sum of the power spectrum [25], [26].

$$f_{\text{mean}_i} = \frac{\sum_{j=1}^{M} f_j \cdot P_j^i}{\sum_{j=1}^{M} P_j^i}, \tag{12}$$

where $M$ is the number of frequency bins, $f_j$ is the frequency value of the EMG power spectrum at frequency bin $j$, and $P_j$ is the EMG power spectrum at frequency bin $j$.

2) *Median frequency* — a frequency at which the EMG power spectrum is divided into two regions with equal integrated power[25], [26]. The halved power spectrum is then traversed and the median frequency is obtained.

$$\sum_{j=\text{f median}}^{M} P_j^i = \frac{1}{2} \cdot \sum_{j=1}^{M} P_j^i, \tag{13}$$

where MDF is the median of the number of frequency bins $M$.

### D. Hidden Markov Model

To take advantage of the patterns produced by fingers while typing, the HMM is employed to predict the fingers that have been pressed given time $t$. A left-to-right Gaussian mixture HMM is built with 6 states: 5 fingers and a transition state, which represents the hand movement as it is between releasing a key and pressing the next key. Figure 4 shows the state transition diagram between the finger and transition states.

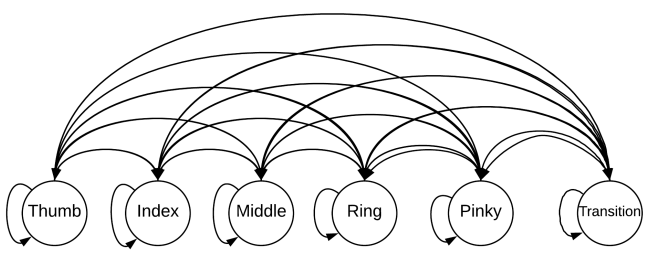


Fig. 4: State transition diagram of the GM-HMM.

A HMM $\lambda = (A, B, \Pi)$ consists of the following:

This article has been accepted for publication in a future issue of this journal, but has not been fully edited. Content may change prior to final publication. Citation information: DOI 10.1109/JSEN.2019.2908312, IEEE Sensors Journal



1) A set of $H$ hidden states, $S = S_1, S_2, ..., S_N$.
2) A state transition probability distribution $A = a_{ij}$ where $i, j \in S$. More formally,

$$a_{ij} = P(S_t = S_j | S_{t-1} = S_i), 1 \leq i, j \leq H \tag{14}$$

3) An observation probability distribution $B = b_i(o_t)$. The probabilistic function for each state $s_i$ is:

$$b_i(o_t) = P(o_t | S_t = S_i) \tag{15}$$

where $o_t$ is the observation at time $t$.
4) An initial probability distribution $\Pi = \pi, i \in S$ where $\pi_i$ is defined as:

$$\pi_i = P(S_1 = S_i) \tag{16}$$

The transition and observation probability distributions $A$ and $B$ are constructed from training data. The state relationships can be thought of as a fully connected graph, in which a state has a non-zero probability of transitioning to any other state as shown in Figure 4. However, due to the abundance of transition states (users are more often in transition than using any other finger) every finger state has a higher probability of transitioning to a transition state than a finger state.

In a GM-HMM, the function $b_i(o_t)$ takes the form of a Gaussian mixture of continuous probability density functions (PDF):

$$b_i(o_t) = \sum_{k=1}^{M} w_{ik} b_{ik}(o_t), i = 1, ..., N \tag{17}$$

where $M$ is the number of mixtures and $w$ is the weight of each mixture. The mixture weights have the following constraints:

$$\sum_{k=1}^{M} w_{ik} = 1; w_{ik} \geq 0, i = 1, ..., N, k = 1, ..., M \tag{18}$$

Each $b_{ik}(o_t)$ is a $d$ dimensional Gaussian density with mean vector $\mu_{ik}$ and covariance matrix $\Sigma_{ik}$. For each state, a multivariate Gaussian density in the form:

$$b_{ik}(o_t) = g(o_t, \mu_{ik}, \Sigma_{ik}) = \frac{1}{\sqrt{((2\pi)^d |\Sigma_{ik}|}} \cdot exp\Big( -\frac{1}{2}(o_t - \mu_{ik})^T \Sigma_{ik}^{-1} (o_t - \mu_{ik}) \Big) \tag{19}$$

is used where $o_t$ is the observation. For each state $s_i$, the mean and covariance $(\mu_i, \Sigma_i)$ are used to construct the emissions matrix. Hence, it is important to choose an appropriate value for $d$ for each state's Gaussian mixture density function, which in turn defines its mean and covariance pairs. To do so, a GMM with different parameters is fit to the observations of each state. The model with the smallest Bayesian Information Criterion (BIC) is selected as the most representative model of the data. Indeed, minimizing the BIC corresponds to maximizing the posterior model probability for a large number of observations and is an effective method of selecting a model [27]. The BIC can be defined as:

$$BIC = -2 \cdot \ln(\hat{\theta}) + p \cdot \ln(n), \tag{20}$$

where $\hat{\theta} = p(\hat{o}|\delta, M)$ is the maximized value of the likelihood function of the model $M$, $p$ is the number of free parameters to be estimated, and $n$ is the number of observations [27].

## V. Experimental Setup

To verify the functionality and fidelity of XTREMIS, its signal is compared to the gold standard in EKG/EMG/EEG data collection: the BioSemi ActiveTwo [7]. Specifically, XTREMIS is compared to BioSemi in two aspects:

1) **Signal quality**: We evaluate the signal of XTREMIS as well as compare it to BioSemi's signal in a salt water experiment to verify their similarity.
2) **GM-HMM classification performance**: We compare XTREMIS to BioSemi in ballistic gesture recognition in a similar experiment to our previous work [8]. In this work, however, the experiment encompasses only anatomically-aware electrode placement using XTREMIS and BioSemi ActiveTwo at the same 1024 Hz sampling rate, whereas the previous work explored a ring-of-electrodes configuration and different sampling rates.

We begin by presenting the signal-level analysis and a signal-to-noise ratio comparison between XTREMIS and BioSemi ActiveTwo, then proceed to show that the highly correlated signal leads to a good ballistic gesture classification accuracy by performing typing experiments on 8 participants: 4 females and 4 males.

### A. Signal Comparison

To verify the SNR of XTREMIS over different frequencies, a signal generator was used to input sine wave signals of varying frequencies at different sampling rates. The SNR was calculated by first applying a notch filter at 60 Hz to eliminate power line noise. The input is then normalized and 5 segments – equally spaced – are extracted from the entire data stream. The measured signal may not always be strictly periodic (due to various potential factors surrounding the experiment), making it more similar to a real biomedical signal. If this irregularity is left unchecked, it will create discontinuities that appear as high frequency components in the fast Fourier transform (FFT). Hence for each segment, a Hann window [28] is extracted to reduce the amplitude of these potential discontinuities. The power-spectral density (PSD) of the signal is then obtained from the FFT using Welch's method [29] since the frequency range of the fundamental frequency of the input signals is known. The SNR is then obtained from the PSD as follows:

$$SNR = 10 \cdot log_{10}\left( \frac{\sum_{i=f_1}^{f_2} P(i)}{\sum_{f_x \in F} P(S) - \sum_{i=f_1}^{f_2} P(i)} \right), \tag{21}$$

where $P(i)$ is the normalized power of the signal between frequencies $f_1$ and $f_2$ and $P(S)$ is the normalized power of the signal at all frequencies.

*1) Saline Experiment:* Since BioSemi ActiveTwo is the gold standard of EKG/EMG/EEG machinery, it is important to ensure that the signal from XTREMIS is similar to the signal from BioSemi. To analyze this, electrodes from a signal generator are placed in two buckets of saline solution (a mixture of sodium chloride with water). The reference electrodes are placed into one bucket(the reference bucket) and the signal electrodes are placed into the other (signal bucket).

The reference electrodes of XTREMIS and BioSemi ActiveTwo are also placed into the reference bucket, while their channel electrodes are placed into the signal bucket. The signal generator then generates a sine wave signal at a predetermined frequency, which is first verified through an oscilloscope to ensure consistency and precision. XTREMIS and BioSemi are configured to collect data from the electrodes submerged in the signal bucket and their signals are then compared. This experimental setup is common in testing EMG equipment due to the similarity in electrical conductivity between the human body and saline. Figure 5 highlights the setup in separating the reference electrodes and the channel electrodes in two separate buckets.

This article has been accepted for publication in a future issue of this journal, but has not been fully edited. Content may change prior to final publication. Citation information: DOI 10.1109/JSEN.2019.2908312, IEEE Sensors Journal



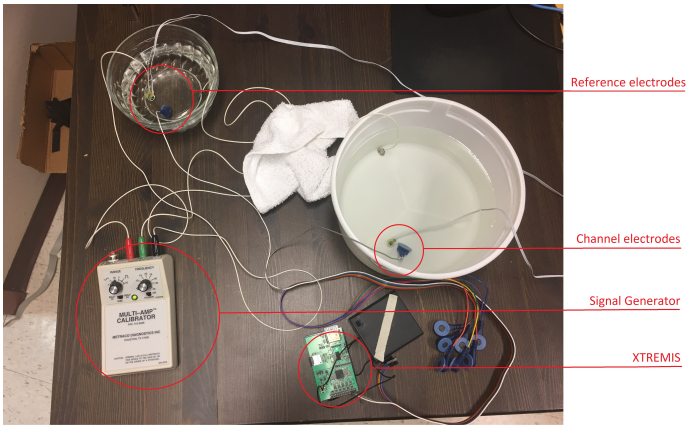


Fig. 5: The setup for the salt water signal comparison test. Reference electrodes from the signal generator, XTREMIS, and BioSemi are placed in the bucket to the top left, while the channel electrodes are placed in the bucket to the right.

### B. Classification Comparison

Finger movement prediction is analyzed during a typing task under 3 different typing speeds: slow, regular, and fast. A 500-word paragraph is presented to the subject. The experimental procedure is as follows:

1) The subject is asked to perform a test run of the paragraph.
2) The subject types the paragraph at slow speed (10-25 words-per-minute).
3) The subject then types the paragraph at their regular typing speed (30-50 words-per-minute).
4) The subject types the paragraph as fast as they can (50-75 words-per-minute).

Additionally, finger movement is analyzed during the typing task under 3 factors:

1) Words-per-minute (WPM).
2) Electrode placement configurations.
3) Sample rates.

The BioSemi and XTREMIS are fitted onto subjects in an alternating fashion such that half the subjects had XTREMIS fit onto them first, and the other half had BioSemi fit first. This acts as a control in case subjects' typing habits change as they type a more familiar paragraph (e.g., they're devoting fewer cognitive resources to reading the paragraph, and hence are more able to exert control over which fingers they're using). It is important to note that both systems used the same type of electrodes – silver/silver chloride. After each time the subject types the paragraph, they have the option of taking a rest to recuperate and ensure they are not too tired to continue. We will first discuss the process of marking ground truth labels for each system.

*1) Automated Collection of Ground Truth Labels:* As discussed in Section III-C, XTREMIS' DMS works similarly to BioSemi's trigger interface. To properly annotate data with key press and key release times, an external trigger system was constructed to translate key events to data markers. Therefore, two systems were built that functioned almost identically: a trigger system for BioSemi, and one for XTREMIS. Each system consisted of a PS/2 keyboard interfaced with an Arduino Uno, which in turn was interfaced with the BioSemi trigger input connector or the DMS on XTREMIS. In a sense, the Arduino functions as a Serial-to-Parallel converter: it receives input from the PS/2 keyboard, converts it to a binary number (8-bits for BioSemi, 6-bits for XTREMIS), and then inputs this number to BioSemi's trigger system or XTREMIS' DMS.

Further, electrodes were placed on the individual's right forearm in an anatomical configuration identified in previous works to be the best placement of electrodes to capture muscular contractions clearly [30], [8].

## VI. Results and Discussion

### A. Signal Quality

Figure 6 shows the SNR of the XTREMIS signal at different sine wave frequencies into one channel of XTREMIS collecting at 1024 Hz.

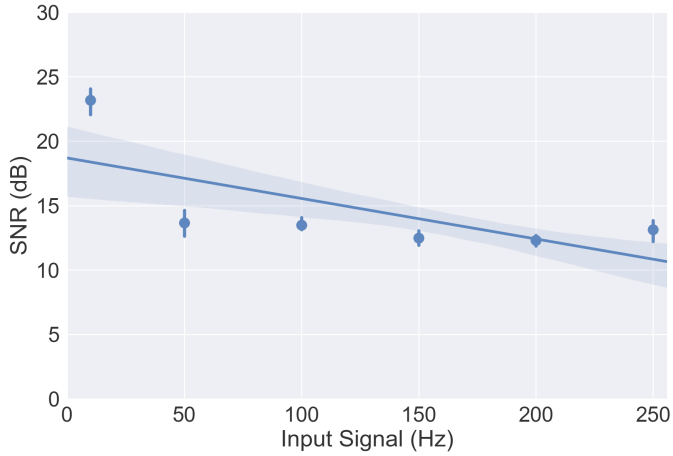


Fig. 6: SNR of XTREMIS signal at different input signal frequencies.

It should be noted that the ADS1299 chip's sample rate becomes less stable at higher frequencies. This is likely due to the design of the ADS1299 chip combined with the small form factor of XTREMIS ($55mm \times 35mm$), as the wires on board may generate high frequency noise that is picked up by the chip. It was found that approximately 1024 Hz is the maximum sampling rate at which the SNR is high enough to obtain a reliable signal at all biosignal wave frequencies. Since the bandwidth of EMG, EEG, and EKG signals is 10-500 Hz [9], 1-50 Hz [31], and 0.05-100 Hz [32] respectively, the signal quality of XTREMIS is still sufficient at high sampling rates to capture more than the Nyquist frequency of the EKG, EEG, and EMG signals.

When sampling at rates higher than 500 Hz and high gains (specifically, a gain of $\times 8$), there is a small shift in the detected frequency of a given signal due to a higher noise. Figure 7 shows the percentage in which the signal frequency shifts at different input signal frequencies while sampling at 1024 Hz. This measure can also be considered as a percent error on the detected signal frequency with different input signals. Since we already know the PSD of the incoming signal, it is possible to calculate the signal frequency shift as follows:

$$shift = 100 \times \frac{f_{max} - f_{input}}{f_{input}}, \tag{22}$$

where $f_{max}$ is the frequency detected by XTREMIS with the highest amplitude and $f_{input}$ is the frequency of the input signal. The similarity in shift percentage at different frequencies indicates that there is a consistency to the frequency shift. This consistency is due to the fact that the ADS1299 chip always samples at its highest frequency (16 kHz) regardless of sample rate. Indeed, changing the sampling rate on the ADS1299 actually changes the decimation ratio, and hence why at higher sampling rates there is a higher

This article has been accepted for publication in a future issue of this journal, but has not been fully edited. Content may change prior to final publication. Citation information: DOI 10.1109/JSEN.2019.2908312, IEEE Sensors Journal



amount of noise due to the reduction in averaging samples. This also corresponds with the ADS1299 data sheet specification regarding the increase of noise if the data rate and the gain setting are set too high. Data rates are to be minimized for each application to reduce noise as much as possible [23].

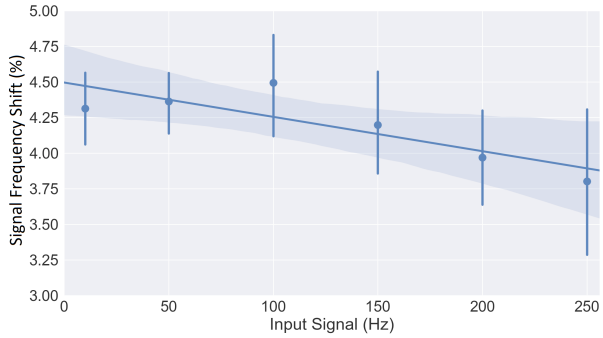


Fig. 7: Shift of XTREMIS signal's frequency at different input signal frequencies.

### B. Signal Comparison

Figure 8 shows the SNR calculated for XTREMIS and for BioSemi ActiveTwo in the saline experiment. The SNR of BioSemi ActiveTwo is – as expected – higher than XTREMIS as it is a research-grade EKG/EEG/EMG machine with more sophisticated and proprietary biomedical technology. More specifically, BioSemi ActiveTwo's electrodes have built-in amplifiers that amplify the signal prior to sending it to the machine – this results in a significantly cleaner signal as the amplification occurs close to the source. In the case of XTREMIS, the amplification occurs on the circuit board – after the signal passes through the wires on its way from the skin. This creates a higher level of noise. However, this creates a tradeoff between cost and signal precision since the state-of-the-art electrodes on BioSemi cost approximately $640 for a 16 channel set, whereas XTREMIS electrodes cost approximately $40. Both systems follow a similar trend in their SNR progression at different frequencies, indicating that XTREMIS is a valid alternative due to its portability, ease-of-use, and robust signal.

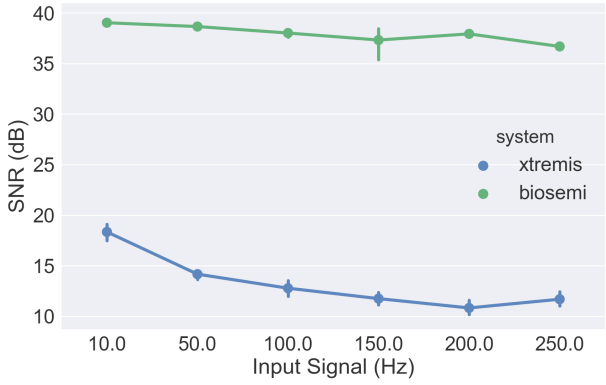


Fig. 8: Comparison between the SNR of XTREMIS and BioSemi ActiveTwo at different input signal frequencies.

### C. Classification Results

We compare the classifier performances averaged over all subjects across different speeds using ground truth labeling described in Section V-B1 and following the experimental procedure discussed in Section V-B. Figure 9(a) shows the average accuracy of all subjects across 3 different speeds while collecting data from BioSemi, XTREMIS, and the Myo armband. The accuracies obtained from applyoing the algorithm using BioSemi data v.s. XTREMIS data suggests that the signal of BioSemi and XTREMIS is similar enough that it is possible to have comparable performance in classification. Further, this result is significantly higher than the highest accuracy achieved by Myo: approximately $82\%$ at the slowest typing speed.

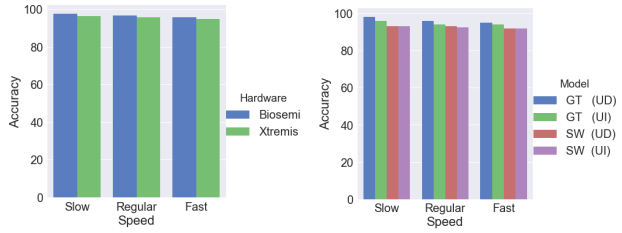


(a) (b)

Fig. 9: (a) GM-HMM accuracy using ground truth data using different hardware. Results averaged over all subjects. (b) XTREMIS Accuracies across User-Dependent and User-Independent GMHMM models

A strong classification model should function across speed as well as users. Figure 9 (b) highlights the performance of the GM-HMM user-independent (UI) model v.s. the user dependent (UD) model on data collected using XTREMIS. The accuracy of UD model reported is the average accuracy from all user trials. The UI GM-HMM generally performs almost as well as its UD counter-part, indicating that the GM-HMM can be trained to function across multiple users using XTREMIS.

Table I highlights the average precision and recall achieved across all users using ground truth data on all systems. The consistent high precision and recall scores across all speeds as well as their similarity between XTREMIS and BioSemi indicate that not only does the GM-HMM function well across speeds, but XTREMIS' performance and data quality collected is similar to BioSemi. On the other hand, the Myo armband's precision and recall suffer due to its lower sample rate and rigid form factor.

Tables II and III are confusion matrices of the GM-HMM trained on BioSemi and XTREMIS, respectively. The GN-HMM suffers most on both devices when classifying between middle and ring fingers. This may be due to the middle and ring fingers sharing several muscles and as a result having a very similar waveform. The lower classification on XTREMIS suggests that the signal quality is a contributing factor to classification, even though the GM-HMM also takes advantage of movement patterns during the training phase.

### D. Configuration Effects

Prior to constructing XTREMIS, we compared the classifier performances averaged over all subjects across different speeds using the ring and anatomical electrode placements using subject dependent training on Myo and BioSemi ActiveTwo. Table IV shows the classification accuracies obtained when typing a paragraph using the Myo with ground truth data.

Tables V and VI show the average performance over all subjects of each classifier for the Biosemi ActiveTwo system in ring and anatomical-based configurations, respectively. The GM-HMM's consistency of performance across speeds and degradation of performance across placements show that electrode placement indeed

This article has been accepted for publication in a future issue of this journal, but has not been fully edited. Content may change prior to final publication. Citation information: DOI 10.1109/JSEN.2019.2908312, IEEE Sensors Journal



TABLE I: Average Precision and Recall when typing a paragraph using XTREMIS v.s. BioSemi ActiveTwo v.s. Myo armband

| | | XTREMIS | | BioSemi | | Myo Armband | |
|---|---|---|---|---|---|---|---|
| | | Precision | Recall | Precision | Recall | Precision | Recall |
| Speed | Slow | 92.4% | 88.2% | 95.2% | 90.2% | 78.16% | 72.31 |
| | Regular | 93.1% | 89.1% | 94.8% | 91.3% | 77.02 | 73.47 |
| | Fast | 91.8% | 89.0% | 93.1% | 89.7% | 74.45 | 64.33 |

TABLE II: Confusion matrix of GM-HMM using XTREMIS

| | | Ground Truth | | | | | |
|---|---|---|---|---|---|---|---|
| | | Thumb | Idx. | Mid. | Ring | Pinky | Tran. |
| Prediction | Thumb | 96% | 0% | 0% | 0% | 0% | 4% |
| | Idx | 0% | 91% | 7% | 0% | 0% | 2% |
| | Mid. | 0% | 0% | 92% | 5% | 0% | 3% |
| | Ring | 0% | 0% | 6% | 94% | 0% | 0% |
| | Pinky | 0% | 0% | 0% | 5% | 92% | 3% |
| | Tran. | 0% | 0% | 0% | 0% | 0% | 100% |

TABLE III: Confusion matrix of GM-HMM using BioSemi ActiveTwo

| | | Ground Truth | | | | | |
|---|---|---|---|---|---|---|---|
| | | Thumb | Idx | Mid. | Ring | Pinky | Tran. |
| Prediction | Thumb | 97% | 0% | 0% | 0% | 0% | 3% |
| | Idx | 0% | 94% | 4% | 0% | 0% | 2% |
| | Mid. | 0% | 0% | 92% | 5% | 0% | 3% |
| | Ring | 0% | 0% | 4% | 95% | 0% | 1% |
| | Pinky | 0% | 0% | 0% | 5% | 93% | 2% |
| | Tran. | 0% | 0% | 0% | 0% | 0% | 100% |

TABLE IV: Classifier performance when typing a paragraph while wearing the Myo armband.

| | | Paragraph Typing | | | |
|---|---|---|---|---|---|
| | | HMM | SVM | kNN | DT |
| WPM | Slow | 82% | 65.3% | 63% | 63.2% |
| | Regular | 82% | 55.3% | 53.1% | 53% |
| | Fast | 80% | 52.3% | 49.8% | 48.1% |
| | Fastest | 78% | 43% | 42.2% | 41% |

TABLE V: Classifier performance when typing a paragraph using the Biosemi ActiveTwo sEMG, with electrodes arranged in a ring configuration like the Myo armband.

| | | Paragraph Typing | | | |
|---|---|---|---|---|---|
| | | HMM | SVM | kNN | DT |
| WPM | Slow | 94% | 72% | 72% | 70% |
| | Regular | 93.2% | 70% | 69.2% | 67% |
| | Fast | 93% | 68% | 66.5% | 64.2% |
| | Fastest | 92.6% | 66.3% | 66% | 64.1% |

plays a role in classification accuracy. Moreover, using a GM-HMM with an anatomical placement of electrodes yields the best results. The confusion matrix in Table II shows that while the HMM with anatomical placement of electrodes performs well, it still suffers most when classifying between middle and ring fingers. This may be due to the middle and ring fingers sharing several muscles and as a result having a very similar waveform. Other classifiers' performance drops significantly as speed increases, likely due to their inability to take advantage of transition probabilities.

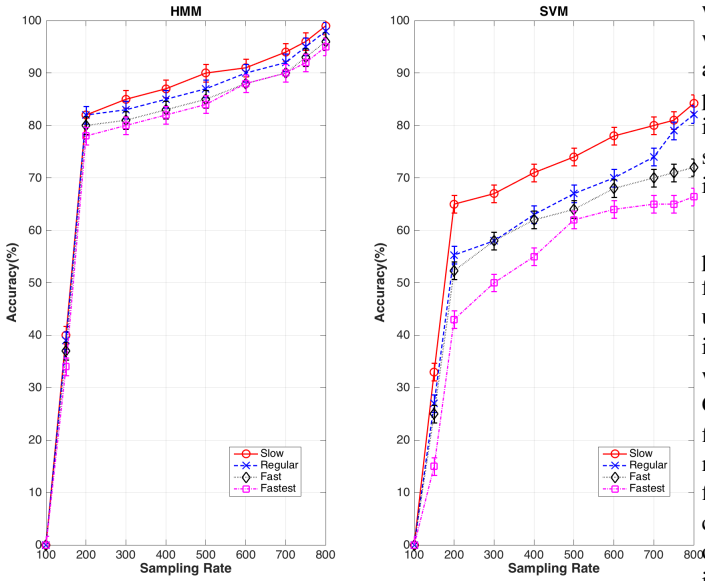


Fig. 10: Classifier accuracy V.S. sampling rate using Biosemi ActiveTwo with anatomical configuration for HMM and SVM.

Additionally, the high performance of the Biosemi ActiveTwo compared to the Myo indicate that sampling rate also plays a role. To verify this, the data obtained from the anatomical placement was downsampled down to approximately 50 Hz and the classifier accuracy was obtained at each sampling rate. Figure 10 shows the changes in HMM and SVM accuracy as sampling rate increases. For both methodologies, a sliding window of 50ms with 10ms overlap was used. Window size and sampling rate are correlated in that if one is sufficiently large, the other must be sufficiently small. In other words, the window size must be larger in order to include more samples for analysis. Similarly, if the sampling rate is high, the window size should be smaller. Due to timing and space constraints, we have not investigated the impact of different window sizes on accuracy, and leave it to future works. Additionally, at 200 Hz the performance becomes comparable to the accuracies achieved by Myo in Table IV. Therefore, this validates the ISEK standard [9] for EMG signal bandwidth as well as confirms that the 200 Hz claimed by Myo is not enough for research-level use.

*1) Onset Detection:* Finally, Figures 11(a) and (b) show a comparison between the timings of classifications for two GM-HMMs for each device: one using ground truth (GT) as training and another using the sliding window (SW) approach. A "too early" classification indicates that the GM-HMM classified a window as a finger when it was still a transition, while a "too late" classification indicates that the GM-HMM classified a window as a transition when it has become a finger already. Finally, a "misclassification" is when the GM-HMM misses a finger movement entirely or classifies a finger as another finger. Therefore, finger detection accuracy is not only defined as correct v.s. incorrect classifications, it is also defined by the *timing* of classifications. Figures 11(a) and (b) indicates that the GM-HMM is more inclined to make a classification too early rather than too late. This can be due to the delay between a muscle contraction and a key press, as humans must first contract the muscles before a movement is made. Additionally, this result is consistent with the timing analysis performed in our previous work [8].

This article has been accepted for publication in a future issue of this journal, but has not been fully edited. Content may change prior to final publication. Citation information: DOI 10.1109/JSEN.2019.2908312, IEEE Sensors Journal



TABLE VI: Classifier performance when typing a paragraph using the Biosemi ActiveTwo sEMG, with electrodes placed on specific muscles as shown in Figure **??**(b)

| | Paragraph Typing | | | |
|---|---|---|---|---|
| **WPM** | HMM | SVM | kNN | DT |
| Slow | 98.4% | 88.2% | 87.4% | 85.2% |
| Regular | 97.1% | 85.1% | 84.2% | 84% |
| Fast | 96.8% | 76% | 74.5% | 74% |
| Fastest | 96.4% | 71% | 69.4% | 68.2% |

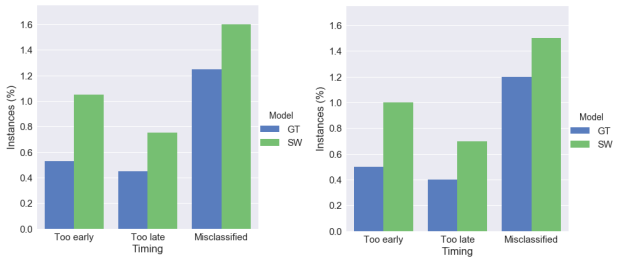


(a) XTREMIS (b) BioSemi ActiveTwo

Fig. 11: Timing of GM-HMM Recognition on BioSemi ActiveTwo and XTREMIS

### *E. Power Consumption Analysis*

Power consumption analysis is an important cornerstone of any embedded system solution. Due to the Wi-Fi SoC and the ADS1299 chip's power consumption, the total power consumption of XTREMIS cannot be strictly classified as "low-power". However, XTREMIS requires only 4 AA batteries connected in series to perform all of its functions. Table VII shows the power consumption and estimated battery life for each operating mode with ADS1299 collecting at 1024 Hz powered by 4 Duracell Procell AA batteries with a capacity of 2148 mAh. These estimates are based on measurements of current and voltage taken under each operating mode, and may not be strictly accurate since the measurements were not performed until the batteries ran out. However they provide a reasonable rough idea of the expected operation time. The most power-hungry mode is streaming over Wi-Fi at 1024 Hz, which lasts approximately 18 hours – which is still long enough for longitudinal studies like sleep studies. Myo, on the other hand, claims a 24 hour battery life while streaming [4]. However, Myo has an unfair advantage in this case as it is using BLE technology to stream at 250 Hz. Since the ADS1299 collects data at a rate of 16 kHz and then decimates it according to the user's chosen data rate, it makes no difference in power consumption to reducing the sampling rate to save power on XTREMIS.

TABLE VII: Power consumption in different modes of operation on XTREMIS

| **Operating Mode** | **Avg. Current(mA)** | **Est. Battery Life** |
|---|---|---|
| Wi-Fi ON (No data collection) | 115.60 | 18 hours 38 minutes |
| Wi-Fi OFF (No data collection) | 87.91 | 24 hours 43 minutes |
| Wi-Fi ON (Data collection and streaming) | 120.43 | 17 hours 45 minutes |
| Wi-Fi OFF (Data collection) | 113.75 | 18 hours 53 minutes |

## VII. Conclusion and Future Works

We presented XTREMIS: a low-cost and portable EMG platform with a similar form factor to off-the-shelf wearable sensors that is comparable to research-grade EMG machines in sampling rates, electrode placement fluidity, and signal-level processing. Indeed, experiments on 8 subjects have shown that not only does XTREMIS functionally outperform off-the-shelf technologies; it also produces a signal that is similar to that of research-grade EMG machines. It is also capable of EKG and EEG signal data collection.

Although XTREMIS currently performs well, it is important to address several issues moving forward. The first is placing it into a more user-friendly form factor: currently it rests as a standalone unit away from the user. A better form factor would be integrating it into a sleeve to be worn by the user. Secondly, to increase usability it is important to explore the use of dry-surface electrodes instead of the current wet-gel silver/silver chloride ones. Dry-surface electrodes will create a noisier signal but eliminate the need to use conductive gel for every experiment, making it more suitable to users not trained in EKG/EMG/EEG data collection. Finally, the sampling rate currently destabilizes at sampling rates above 500 Hz. We have shown that this is due to the ADS1299 chip's design, however it would be interesting to explore some post-hoc processing steps that may be implemented to overcome this issue and increase the SNR even further at higher frequencies. On the other hand, a better form factor that separates digital and analog signals in a more effective way is also being explored. Finally, it is important to upgrade the DMS system to map all possible letters on a keyboard, potentially making the entire system language-agnostic. The current implementation only supports 6 bits for markers due to the pin number of pins available for marking on the current iteration of XTREMIS. Indeed, in addition to an additional number of general-purpose input/output pins.

## References

[1] G. Robertson, G. Caldwell, J. Hamill, G. Kamen, and S. Whittlesey, *Research methods in biomechanics, 2E*. Human Kinetics, 2013.

[2] K. Farry, I. Walker, and R. Baraniuk, "Myoelectric teleoperation of a complex robotic hand," *Robotics and Automation, IEEE Transactions on*, vol. 12, no. 5, pp. 775–788, Oct 1996.

[3] X. Chen and Z. J. Wang, "Pattern recognition of number gestures based on a wireless surface emg system," *Biomedical Signal Processing and Control*, vol. 8, no. 2, pp. 184–192, 2013.

[4] (2016) Myo gesture control armband - wearable technology by thalmic labs. https://www.myo.com. Accessed: 2016-03-30.

[5] Athos muscle activity measurement fitness apparel. https://www.liveathos.com. Accessed: 2017-07-31.

[6] Hexoskin smart monitor. https://www.hexoskin.com. Accessed: 2017-07-31.

[7] Biosemi activetwo multi-modal data acquisition system with active electrodes. https://biosemi.com. Accessed: 2017-07-31.

[8] A. Shaabana, R. Zheng, J. Legere, and M. v. Mohrenschildt, "Finger movement recognition during ballistic movements using electromyography," in *Proceedings of the Second IEEE/ACM conference on Connected health: Applications, Systems and Engineering technologies*. IEEE, 2017, pp. 302–311.

[9] R. Merletti and P. Di Torino, "Standards for reporting emg data," *Journal of Electromyography and Kinesiol*, vol. 9, no. 1, pp. 3–4, 1999.

[10] T. Starner, J. Weaver, and A. Pentland, "Real-time american sign language recognition using desk and wearable computer based video," *IEEE Transactions on Pattern Analysis and Machine Intelligence*, vol. 20, no. 12, pp. 1371–1375, 1998.

[11] S. Mitra and T. Acharya, "Gesture recognition: A survey," *Systems, Man, and Cybernetics, Part C: Applications and Reviews, IEEE Transactions on*, vol. 37, no. 3, pp. 311–324, 2007.

[12] R. Rosenberg, "The biofeedback pointer: Emg control of a two dimensional pointer," in *Digest of Papers. Second International Symposium on Wearable Computers (Cat. No.98EX215)*, Oct 1998, pp. 162–163.

[13] R. A. R. C. Gopura, K. Kiguchi, and Y. Li, "Sueful-7: A 7dof upper-limb exoskeleton robot with muscle-model-oriented emg-based control," in *2009 IEEE/RSJ International Conference on Intelligent Robots and Systems*, Oct 2009, pp. 1126–1131.

[14] F. Pareschi, P. Albertini, G. Frattini, M. Mangia, R. Rovatti, and G. Setti, "Hardware-algorithms co-design and implementation of an analog-to-information converter for biosignals based on compressed sensing," *IEEE transactions on biomedical circuits and systems*, vol. 10, no. 1, pp. 149–162, 2016.

[15] H. G. Stack, "Muscle function in the fingers," *Journal of Bone & Joint Surgery, British Volume*, vol. 44, no. 4, pp. 899–909, 1962.

[16] *TPD4E1B06 4-Channel Ultra Low Leakage ESD Protection Device*, Texas Instruments, 2014.

[17] K. R. Wheeler, "Device control using gestures sensed from emg," in *Soft Computing in Industrial Applications, 2003. SMCia/03. Proceedings of the 2003 IEEE International Workshop on*. IEEE, 2003, pp. 21–26.

[18] G. Kaur, A. S. Arora, and V. Jain, "Comparison of the techniques used for segmentation of emg signals," in *Proceedings of the 11th WSEAS international conference on Mathematical and computational methods in science and engineering*. World Scientific and Engineering Academy and Society (WSEAS), 2009, pp. 124–129.

[19] X. Zhang, X. Chen, W.-h. Wang, J.-h. Yang, V. Lantz, and K.-q. Wang, "Hand gesture recognition and virtual game control based on 3d accelerometer and emg sensors," in *Proceedings of the 14th international conference on Intelligent user interfaces*. ACM, 2009, pp. 401–406.

[20] G. Kondo, R. Kato, H. Yokoi, and T. Arai, "Classification of individual finger motions hybridizing electromyogram in transient and converged states," in *Robotics and Automation (ICRA), 2010 IEEE International Conference on*, May 2010, pp. 2909–2915.

[21] B. Hudgins, P. Parker, and R. N. Scott, "A new strategy for multifunction myoelectric control," *Biomedical Engineering, IEEE Transactions on*, vol. 40, no. 1, pp. 82–94, 1993.

[22] M. Reaz, M. Hussain, and F. Mohd-Yasin, "Techniques of emg signal analysis: detection, processing, classification and applications," *Biological procedures online*, vol. 8, no. 1, pp. 11–35, 2006.

[23] *ADS1299-x Low-Noise, 4-, 6-, 8-Channel, 24-Bit, Analog-to-Digital Converter for EEG and Biopotential Measurements*, Texas Instruments, 7 2017, rev.C.

[24] M. P. Mobarak, M. J. G. Salgado, R. M. Guerrero, and V. L. Dorr, "Transient state analysis of the multichannel emg signal using hjorth's parameters for identication of hand movements," in *International Multi-Conference on Computing in the Global Information Technology, ICCGI 2014*, 2014.

[25] M. A. Oskoei, H. Hu, and J. Q. Gan, "Manifestation of fatigue in myoelectric signals of dynamic contractions produced during playing pc games," in *Engineering in Medicine and Biology Society, 2008. EMBS 2008. 30th Annual International Conference of the IEEE*. IEEE, 2008, pp. 315–318.

[26] A. Phinyomark, P. Phukpattaranont, and C. Limsakul, "Feature reduction and selection for emg signal classification," *Expert Systems with Applications*, vol. 39, no. 8, pp. 7420–7431, 2012.

[27] E. Wit, E. v. d. Heuvel, and J.-W. Romeijn, "All models are wrong...: an introduction to model uncertainty," *Statistica Neerlandica*, vol. 66, no. 3, pp. 217–236, 2012.

[28] F. J. Harris, "On the use of windows for harmonic analysis with the discrete fourier transform," *Proceedings of the IEEE*, vol. 66, no. 1, pp. 51–83, 1978.

[29] P. Welch, "The use of fast fourier transform for the estimation of power spectra: a method based on time averaging over short, modified periodograms," *IEEE Transactions on audio and electroacoustics*, vol. 15, no. 2, pp. 70–73, 1967.

[30] Y. Itoh, H. Uematsu, F. Nogata, T. Nemoto, A. Inamori, K. Koide, and H. Matsuura, "Finger curvature movement recognition interface technique using semg signals," *Journal of Achievements in Materials and Manufacturing Engineering*, vol. 23, no. 2, pp. 43–46, 2007.

[31] S. Sanei and J. A. Chambers, *EEG signal processing*. John Wiley & Sons, 2013.

[32] J. Webster, *Medical instrumentation: application and design*. John Wiley & Sons, 2009.